

GeV gamma-ray emission from pulsar wind nebula HESS J1356-645 with *Fermi*-LAT

XI LIU,¹ XIAOLEI GUO,¹ YULIANG XIN,¹ FENGRONG ZHU,¹ AND SIMING LIU¹

¹*School of Physical Science and Technology, Southwest Jiaotong University, Chengdu 610031, China; xlguo@swjtu.edu.cn*

ABSTRACT

HESS J1356-645 is considered to be a pulsar wind nebula (PWN) associated with the pulsar PSR J1357-6429. We reanalyze the GeV gamma-ray emission in the direction of HESS J1356-645 with more than 13 years of *Fermi* Large Area Telescope (LAT) data. The extended gamma-ray emission above 5 GeV is found to be spatially coincident with HESS J1356-645. The spectrum in the energy range of 1 GeV-1 TeV can be described by a power law with an index of $\Gamma = 1.51 \pm 0.10$. The broadband spectrum of HESS J1356-645 can be reproduced by a leptonic model with a broken power-law electronic spectrum. In addition, we found evidence that the morphology of the GeV emission from HESS J1356-645 varies with energy, a behavior which is similar to that of the PWN Vela-X. More broadband observations will be helpful to study the energy-dependent characteristics of HESS J1356-645.

Keywords: gamma rays: general — ISM: individual objects (HESS J1356-645) — methods: data analysis

1. INTRODUCTION

More than two hundred very-high-energy (VHE; > 100 GeV) gamma-ray sources have been detected¹, and PWN is the largest population of the identified VHE sources. Remarkably, Cao et al. (2021) reported the detection of ultra-high-energy (UHE; > 100 TeV) gamma-ray emission from 12 Galactic gamma-ray sources. It is notable that there are one or more pulsars within most of the regions around the 12 UHE sources, indicating that the UHE gamma-ray emission possibly originates from PWN. PWNe are important cosmic-ray (CR) accelerators, and the study of gamma-ray emission from PWNe is crucial for exploring the origin of Galactic CRs.

HESS J1356-645 was first discovered by H.E.S.S. (Renaud et al. 2008; H. E. S. S. Collaboration et al. 2011), which is likely associated with the pulsar PSR J1357-645. HESS J1356-645 is an extended gamma-ray source with $\sigma = (0.2 \pm 0.02)^\circ$ for a Gaussian model in the TeV band. The spectrum can be well fitted by a power law with a photon index of $\Gamma = 2.2 \pm 0.2_{\text{stat}} \pm 0.2_{\text{sys}}$ in the energy range of 1 - 20 TeV. And PSR J1357-6429 is a young (characteristic age $\tau_c = 7.3$ kyr) energetic pulsar with a spin-down luminosity of $\dot{E} = 3.1 \times 10^{36}$ erg s⁻¹. The distance is estimated to be 2.5 kpc based on the dispersion measure (Camilo et al. 2004). In addition, Danilenko et al. (2012) found a possible optical counterpart of PSR J1357-6429, and an extremely high transverse velocity in the range of 1600 – 2000 km s⁻¹ was inferred. However, Kirichenko et al. (2015) gave a 90% upper limit of 1200 km s⁻¹ with the observation of Australia Telescope Compact Array (ATCA) at 2.1 GHz.

In the radio band, Duncan et al. (1997) reported a supernova remnant (SNR) candidate G309.8-2.8 located only $\sim 0.1^\circ$ away from HESS J1356-645 with an extension of $15' \times 35'$ at 2.4 GHz. The Parkes-MIT-NRAO (PMN) 4.85 GHz survey and Molonglo Galactic Plane Survey (MGPS-2) at 843 MHz also detected this SNR candidate with the extended structure (Griffith & Wright 1993; Murphy et al. 2007). According to the flux densities, H. E. S. S. Collaboration et al. (2011) fitted the radio spectrum using a power law with a slope of $\alpha = 0.01 \pm 0.07$. Such a flat radio spectrum is much different from that of the typical shell-type SNRs, but is within the values of indices from PWNe (Green 2009; Gaensler & Slane 2006). Esposito et al. (2007) and Zavlin (2007) carried out the X-ray observations with *XMM-Newton* and *Chandra*, and found that the spectrum of the pulsar can be described by a power-law plus blackbody model. At the same time, Zavlin (2007) reported a faint tail-like PWN associated with PSR J1357-6429 using *Chandra* High-

¹ <http://tevcat2.uchicago.edu/>

Resolution Camera (HRC-S) observation, which was also confirmed by Lemoine-Goumard et al. (2011) with *Chandra* ACIS-I data. Analyses of *ROSAT*/PSPC and *XMM-Newton* data revealed a faint extended X-ray structure, which is coincident with the VHE gamma-ray emission (H. E. S. S. Collaboration et al. 2011). Furthermore, Chang et al. (2012) performed deeper observations with *Chandra* ACIS and *XMM-Newton* EPIC data. They reported that the X-ray emission consists of a brighter, compact PWN and a surrounding fainter, but more extended PWN. The spectral slope of the compact component is 1.3 ± 0.3 , while a slope of 1.7 ± 0.2 is obtained for the extended component. While Izawa et al. (2015) tried to investigate the spatial variation of the X-ray photon index from the extended emission, no significant variation was found as a function of the distance from the pulsar.

Lemoine-Goumard et al. (2011) detected the GeV gamma-ray pulsations from PSR J1357-6429, and found this emission has a spectral cutoff at a low energy of ~ 800 MeV. While Lemoine-Goumard et al. (2011) and H. E. S. S. Collaboration et al. (2011) also searched for the GeV gamma-ray counterpart of HESS J1356-645 with *Fermi*-LAT, no significant GeV emission was detected. Acero et al. (2013) reported the detection of a faint GeV counterpart of HESS J1356-645 with a significance of 4.7σ , which is insufficient to perform a more detailed analysis.

In this work, we perform a complete analysis of this region with more than 13-years *Fermi*-LAT data. In Section 2, we present the processes and results of data analysis. In Section 3 we discuss the non-thermal radiation model, based on the multi-wavelength observations. And the conclusion of this work is given in Section 4.

2. DATA ANALYSIS

In this work, we used the latest Pass 8 version of *Fermi*-LAT data² recorded from August 5, 2008 (Mission Elapsed Time 239587201) to January 5, 2022 (Mission Elapsed Time 663033605). The data of ‘‘SOURCE’’ type (evclass=128 and evtype=3) with energy range from 5 GeV to 1 TeV was selected, and filtered with the recommendation of (DATA_QUAL > 0) && (LAT_CONFIG == 1). The region of interest (ROI) is a circle with a radius of 8° centered at the central position of HESS J1356-645 (R.A. = 209 $^\circ$ 0, decl. = -64° 5). The data were binned into 23 logarithmic energy bins, and 100×100 spatial bins with a pixel of 0° 1. To exclude the influence of the Earth Limb, the events with zenith angle greater than 90° were eliminated. For the data analysis, we used the *Fermitools* version 2.0.8³ to carry out the analysis, and the instrument response function P8R3_SOURCE_V3. The Galactic diffuse emission gll_iem_v07.fits and isotropic diffuse background iso_P8R3_SOURCE_V3_v1.txt provided by the Fermi Science Support Center⁴(FSSC) were considered in the analysis. In addition to the two diffuse backgrounds, the model also includes the sources listed in the LAT 12-year source catalog (4FGL-DR3; *Fermi*-LAT collaboration et al. 2022) within the ROI. During the analysis process, the spectral parameters of sources located inside the ROI and the normalizations of the diffuse backgrounds were left free. The standard binned likelihood method was applied to find the parameters of the sources.

2.1. Results

We first generated a $2^\circ \times 2^\circ$ TS map centered at HESS J1356-645, after subtracting the 4FGL-DR3 sources (except for HESS J1356-645) and the diffuse backgrounds, which is shown in Figure 1. Here, the TeV (H. E. S. S. Collaboration et al. 2011) and 4.85 GHz radio observations of HESS J1356-645 are presented as the magenta and cyan contours, respectively. The TS map shows that the GeV gamma-ray emission in the direction of HESS J1356-645 is in a good spatial consistence with the TeV and radio observations, suggesting a common origin.

2.1.1. Spatial Analysis

As shown in Figure 1, there is a discrepancy between the GeV gamma-ray emission we detected and the spatial model used in 4FGL-DR3 catalog. Therefore, we re-analyzed the extension with an uniform disk and a two dimensional (2D) Gaussian models using *fermipy* (Wood et al. 2017). For the analysis of extension, the spectral indices of HESS J1356-645 and nearby sources were fixed to be the best-fit values obtained in the full energy range, while the normalizations of these sources and the diffuse backgrounds were left free. In addition, the radio image at 4.85 GHz and the H.E.S.S. TeV image were also tested as spatial templates. The results of spatial analysis are given in Table 1. We found that the 2D Gaussian model with a 68% containment radius (r_{68}) of 0° 366 is better to describe the GeV gamma-ray emission from HESS J1356-645, and the corresponding TS value is 109. Based on the Akaike infotmation criterion (AIC; Akaike 1974)⁵, we compared the different spatial models. For 2D Gaussian model, the values of Δ AIC are calculated to be

² <https://fermi.gsfc.nasa.gov/ssc/data>

³ <https://fermi.gsfc.nasa.gov/ssc/data/analysis/software/>

⁴ <https://fermi.gsfc.nasa.gov/ssc/data/access/lat/BackgroundModels.html>

⁵ AIC= $-2\ln\mathcal{L}+2k$, where \mathcal{L} is the value of maximum likelihood and k is the parameter numbers of model.

Table 1. Best-fit morphological parameters of HESS J1356-645 with the data above 5 GeV.

Spatial Model	R.A.	decl.	Extension r_{68}	TS	ΔAIC
2D Gaussian	$208^{\circ}614 \pm 0^{\circ}046$	$-64^{\circ}437 \pm 0^{\circ}046$	$0^{\circ}366^{+0^{\circ}045}_{-0^{\circ}040}$	109	7.9
Uniform Disk	$208^{\circ}604 \pm 0^{\circ}029$	$-64^{\circ}413 \pm 0^{\circ}031$	$0^{\circ}332^{+0^{\circ}021}_{-0^{\circ}021}$	96	4.2
H.E.S.S. Image	-	-	-	86	-16.9
Radio Image	-	-	-	78	-9.3

$\Delta\text{AIC} = \Delta\text{AIC}_0 - \Delta\text{AIC}_{\text{gaus}} = 7.9$ and for disk model $\Delta\text{AIC} = 4.2$, where ΔAIC_0 represents the ΔAIC value for the model of HESS J1356-645 in 4FGL. And the values of ΔAIC for H.E.S.S. and radio images are less than zero. The different values of ΔAIC suggest the Gaussian model to be the best-fit spatial template. The r_{68} of the 2D Gaussian template is plotted as a yellow dashed circle in Figure 1, together with the extension in 4FGL-DR3 given by the analysis of Fermi-LAT extended Galactic sources (FGES; Ackermann et al. 2017). The discrepancy between them could be attributed to the different energy ranges, the improved Galactic diffuse model and more observational data used here. In the following spectral analysis, the 2D Gaussian model is adopted as the spatial template of the GeV emission from HESS J1356-645 in order to perform a more detailed analysis.

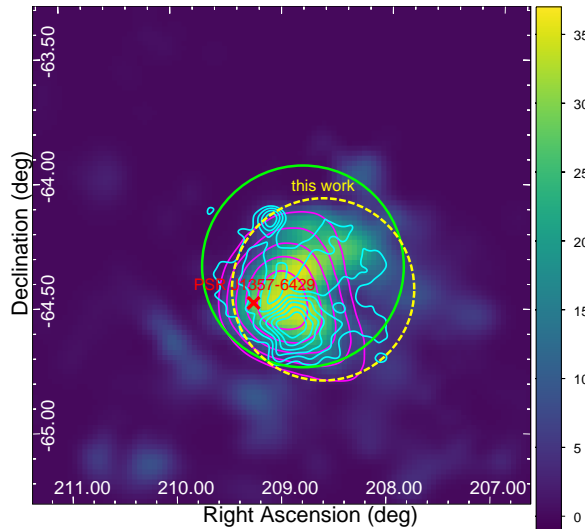


Figure 1. $2^{\circ} \times 2^{\circ}$ TS map centered on HESS J1356-645 with the data above 5 GeV, which is smoothed with a Gaussian width of $0^{\circ}.1$. The yellow dashed and the green solid circles show the best-fit r_{68} of the 2D Gaussian model analyzed in this work and the radius of the uniform disk template used in 4FGL-DR3, respectively. The magenta and cyan contours represent the H.E.S.S. and 4.85 GHz radio observations (H. E. S. S. Collaboration et al. 2011; Griffith & Wright 1993), respectively. And the red cross marks the position of PSR J1357-6429 (Camilo et al. 2004).

To further explore any energy-dependent morphological characteristics of HESS J1356-645, we also performed the localization and extension analyses separately in the energy ranges of 10-100 GeV and 100-1000 GeV. And the data below 10 GeV were not included to minimise the effect of point-spread function (PSF) and diffuse background emission in the low energy band. The analysis procedure is similar to the previous spatial analysis of the full energy band, and the extension is estimated by fitting a 2D Gaussian model. Table 2 contains the results of extension measurements in the two energy bands, and the corresponding TS maps are shown in Figure 2. While the extensions of both energy ranges are comparable, the central position is about $0^{\circ}.2$ away from each other, and both of the central positions are offset from PSR 1357-6429. In addition, we noted that the GeV gamma-ray emission moves toward northwest with energy increasing, indicating the different radiation regions.

And we found that the spectrum of higher energy band is harder than that of lower energy range. However, since the gamma-ray emission is not bright enough to perform a more detailed analysis, the statistical errors are relatively

large, and the variation is possibly caused by the fluctuation of relatively weak signal or the effect of the PSF. Thus, more gamma-ray observational data is desired to study the energy-dependent behavior of HESS J1356-645.

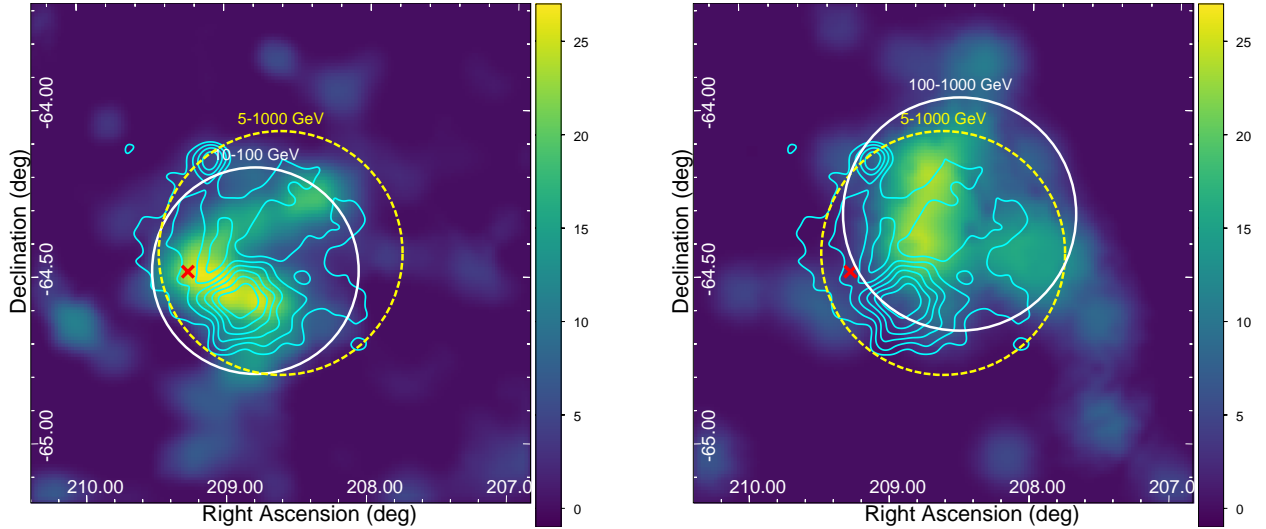


Figure 2. $1^{\circ}5 \times 1^{\circ}5$ TS maps in the energy range of 10-100 GeV (left) and 100-1000 GeV (right). The yellow dashed circle shows r_{68} of HESS J1356-645 for the data above 5 GeV in this work, and the white solid circles represent r_{68} of the Gaussian templates of the two energy bands. The cyan contours represent the 4.85 GHz radio observation (Griffith & Wright 1993). And the red cross shows the position of PSR J1357-6429 (Camilo et al. 2004).

Table 2. The results of energy-dependent extension measurements of HESS J1356-645.

Energy range	Offset ^a	Best-fit position (R.A., decl.)	Extension r_{68}	TS	Γ
10 GeV - 100 GeV	0 $^{\circ}$ 14	(208 $^{\circ}$ 79 \pm 0 $^{\circ}$ 05, -64 $^{\circ}$ 49 \pm 0 $^{\circ}$ 05)	0 $^{\circ}$ 31 $^{+0^{\circ}06}_{-0^{\circ}05}$	55	1.37 \pm 0.27
100 GeV - 1 TeV	0 $^{\circ}$ 47	(208 $^{\circ}$ 50 \pm 0 $^{\circ}$ 07, -64 $^{\circ}$ 32 \pm 0 $^{\circ}$ 08)	0 $^{\circ}$ 35 $^{+0^{\circ}07}_{-0^{\circ}06}$	45	1.08 \pm 0.41

^aThe offset of the centroid of 2D-Gaussian model from the pulsar position.

2.1.2. Spectral Analysis

To derive the spectral energy distribution (SED), we performed the global fit from 1 GeV to 1 TeV. The spectrum of HESS J1356-645 can be well fitted by a power law with a spectral index of $\Gamma = 1.51 \pm 0.10$ and the integrated photon flux is $(5.74 \pm 0.75) \times 10^{-10}$ photons $\text{cm}^{-2} \text{s}^{-1}$. We also tested the log-parabola spectrum for HESS J1356-645, and the value of $\Delta\text{AIC} = \text{AIC}_{\text{Logpb}} - \text{AIC}_{\text{PL}}$ is calculated to be 2.18, where $\text{AIC}_{\text{Logpb}}$ and AIC_{PL} are the AIC values for log-parabola and power-law models, respectively. This result suggests no significant curvature for the gamma-ray spectrum of HESS J1356-645. Then, the data were divided into 6 logarithmic energy bins. And for each energy bin, the likelihood analysis was repeated. During the analysis process, only the normalizations of sources within the ROI and the diffuse backgrounds were set free, while the spectral indices were fixed to be the best-fit values given in the global fit. And an upper limit of 95% confidence level was calculated in the energy bin from 1 GeV to 3.1 GeV, where the TS value of HESS J1356-645 is smaller than 4. The SED is shown in Figure 3, which shows that the GeV SED could connect with the TeV spectrum smoothly. We also estimated the systematic errors due to the Galactic diffuse emission by changing the normalization of the best-fit Galactic diffuse model artificially by $\pm 6\%$ as in Abdo et al. (2010). The sums of statistical and systematic errors are calculated by $\sigma = \sqrt{\sigma_{\text{stat}}^2 + \sigma_{\text{sys}}^2}$, which are shown as the black error bars in Figure 3.

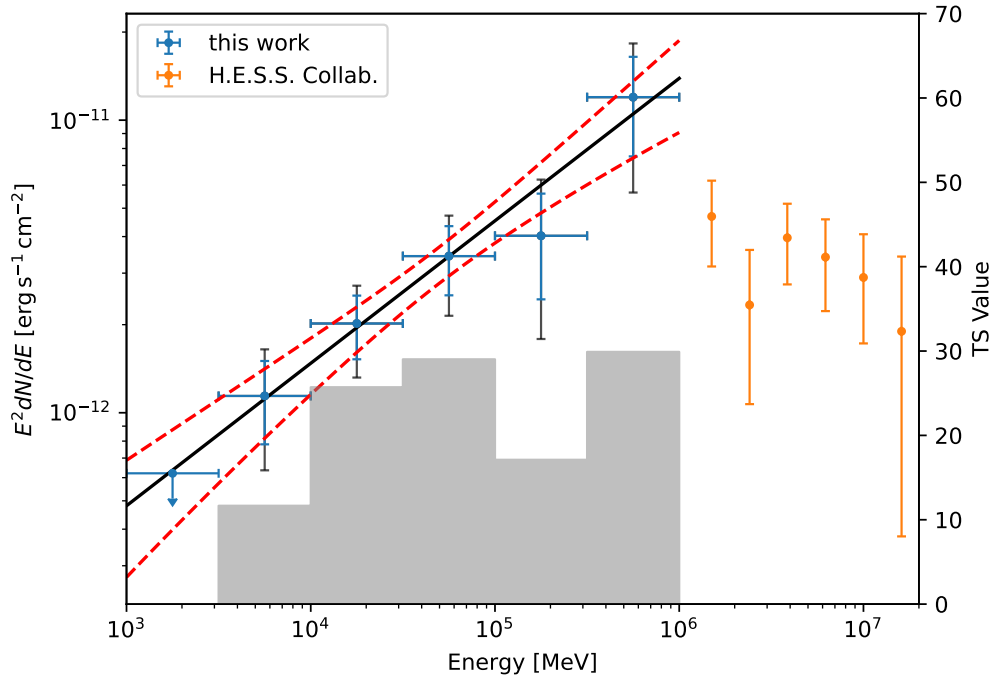


Figure 3. SED of HESS J1356-645. The blue dots are the results of *Fermi*-LAT data with statistical errors in this work, and the black bars mark the sums of the statistical and systematic errors considering the influence of the Galactic diffuse emission model. The best-fit power-law spectrum for the data above 1 GeV and the corresponding statistical error are shown as black solid and the red dashed lines, respectively. The TS value of each energy bin is denoted as the gray histogram. The VHE SED is plotted as the orange dots (H. E. S. S. Collaboration et al. 2011)

Table 3. Model parameters

model	W_e (10^{47} erg)	Γ_1	Γ_2	E_b (TeV)	E_c (TeV)	B (μG)	χ^2
Model A	$4.60^{+0.51}_{-0.40}$	$2.37^{+0.06}_{-0.06}$	$2.75^{+0.19}_{-0.15}$	$5.39^{+1.26}_{-0.95}$	—	$3.61^{+0.59}_{-0.40}$	14.6/12
Model B	$5.08^{+0.51}_{-0.54}$	$2.33^{+0.06}_{-0.06}$	$2.86^{+0.15}_{-0.18}$	$6.35^{+1.61}_{-1.53}$	—	$3.54^{+0.52}_{-0.45}$	14.2/12
Model C	$5.19^{+0.66}_{-0.55}$	$2.45^{+0.01}_{-0.02}$	—	—	567^{+384}_{-221}	$2.92^{+0.29}_{-0.22}$	19.2/12

3. DISCUSSION

Based on the results of *Fermi*-LAT data analysis, the extended GeV gamma-ray source is in spatial coincidence with HESS J1356-645. And the GeV gamma-ray spectrum connects smoothly with the TeV spectrum of HESS J1356-645, which all support the GeV gamma-ray source as to be the low-energy counterpart of HESS J1356-645. For the origin of the gamma-ray emission from HESS J1356-645, the SNR candidate G309.8-2.8 inside this region is considered. However, its flat radio spectrum ($\alpha = 0.01 \pm 0.07$) is much different from that of shell-type SNRs, whose typical indices are ~ 0.5 (Green 2009), but is similar to that of PWNe ($-0.3 \lesssim \alpha \lesssim 0$; Gaensler & Slane 2006). Meanwhile, the nearby pulsar PSR J1357-6429 is energetic enough to power a gamma-ray PWN, compared to other gamma-ray emitting PWNe (Mattana et al. 2009; Acero et al. 2013). Therefore, we suggest that the PWN scenario is favored for the gamma-ray emission from HESS J1356-645.

For a typical PWNe, the emission from radio to X-ray band is produced by the synchrotron radiation of relativistic electrons, while the gamma-ray emission is generally due to the inverse-Compton scattering (ICS) of electrons (leptonic

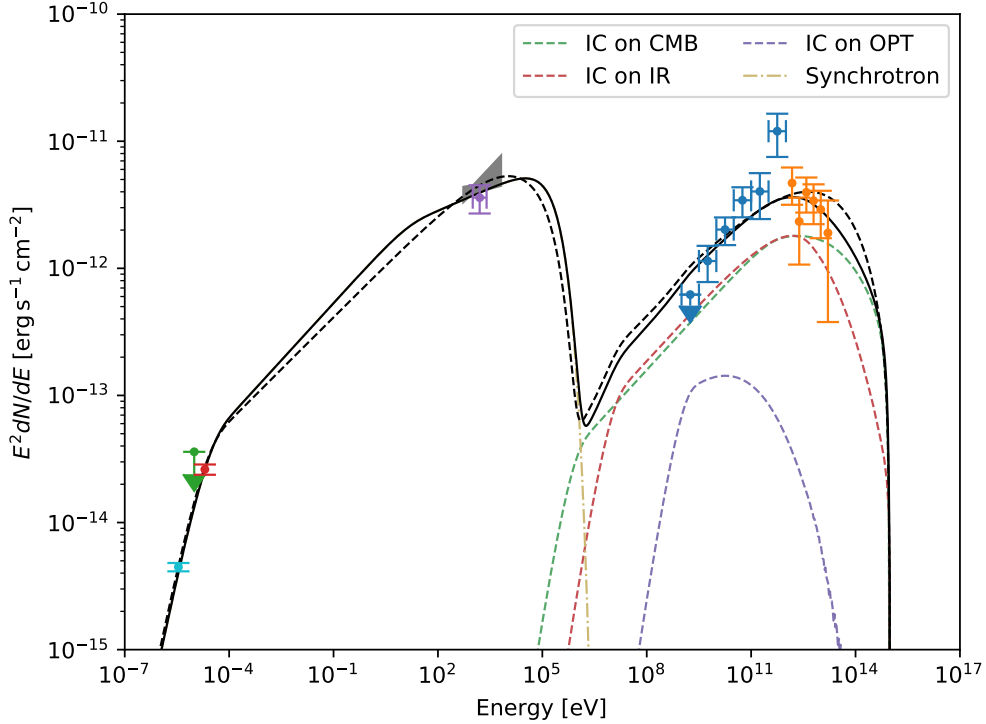


Figure 4. Leptonic model for HESS J1356-645. The broadband emission with model A and model C are represented by the black solid and dashed lines, respectively. The dashed lines of the different colors denote the different radiation components in model A. The radio, X-ray, and TeV gamma-ray data are taken from *H. E. S. S. Collaboration et al. (2011)*. The radio data include the measurements from MGPS-2 at 843 MHz (cyan dot), Parkes at 2.4 GHz (green upper limit) and PMN at 4.85 GHz (red dot). The purple dot and gray butterfly denote the X-ray observations from *ROSAT/SPSC* and *XMM-Newton*, respectively.

model). To constrain the radiation mechanism of HESS J1356-645, a simple one-zone leptonic model is considered. The electron spectrum is assumed to be a broken power law (BPL; *Bucciantini et al. 2011*),

$$\frac{dN}{dE} \propto \begin{cases} \left(\frac{E}{E_b}\right)^{-\Gamma_1}, & E < E_b \\ \left(\frac{E}{E_b}\right)^{-\Gamma_2}, & E > E_b \end{cases}$$

where E_b is the break energy, and Γ_1 and Γ_2 are the spectral indices in the low energy and high energy, respectively. And the maximum energy of electrons is set to be 1 PeV, which results in the high energy cutoff.

Considering the association of PSR J1357-6429, a distance of 2.5 kpc is adopted (*Camilo et al. 2004*). We consider two sets of background photon fields during the multi-wavelength fitting. Model A is comprised of the cosmic microwave background (CMB), the Galactic infrared (IR; the temperature of $T = 35$ K and the energy density of $u = 0.66$ eV cm^{-3}) component and optical ($T = 4600$ K and $u = 0.94$ eV cm^{-3}) emission (*H. E. S. S. Collaboration et al. 2011*). And in model B, the IR and optical photon fields are adopted with the values of $T = 25$ K & $u = 0.4$ eV cm^{-3} and $T = 5000$ K & $u = 0.5$ eV cm^{-3} , respectively. The multi-wavelength data are fitted by *naima* package (*Zabalza 2015*) with the Markov Chain Monte Carlo (MCMC) algorithm. And the derived parameters are shown in Table 3.

For the leptonic model with BPL spectrum, both model A and B can reproduce the multi-wavelength data, and the corresponding broadband SED of model A is shown in Figure 4. The spectral indices of electrons are 2.37 and 2.75, and the break energy is fitted to be ~ 5.4 TeV. When we fitted the broadband spectrum, we noted that a low energy cutoff of ~ 10 GeV is needed to explain the radio data. Considering the flat radio spectrum ($\alpha = 0.01 \pm 0.07$), the spectral index below the break will be $\Gamma = 2\alpha + 1 \sim 1.02$, which is not reasonable for the particle acceleration in PWNe (*Sironi et al. 2015*). Therefore, a low energy cutoff of ~ 10 GeV for the electronic spectrum is considered, which is similar to the result of *H. E. S. S. Collaboration et al. (2011)*. The magnetic field strength is fitted to be

$B \sim 3.7 \mu\text{G}$, which is typical for PWNe (Acero et al. 2013; Torres et al. 2014). And the total energy of electrons above 10 GeV is estimated to be $W_e \sim 4.6 \times 10^{47}$ erg. The corresponding synchrotron cooling timescale of the energy of E_b is $\tau_{\text{syn}} \simeq 1.56 \times 10^2 \left(\frac{E_b}{5 \text{ TeV}}\right) \left(\frac{B}{4 \mu\text{G}}\right)^{-2}$ kyr, which is much larger than the characteristic age of PSR J1357-6429 ($\tau_c \sim 7.3$ kyr). In addition, the variation of spectral index of electrons predicted by synchrotron cooling is ~ 1.0 , while the fitting gives the value of $\Delta\Gamma$ to be about 0.5. Therefore, the break energy may be intrinsic for the electron spectrum injected in PWN instead of being produced by the radiation loss (de Jager 2008).

The electron spectrum following a power law with an exponential cutoff (PLEC; model C), $dN/dE \propto (E/E_0)^{-\Gamma_1} \exp(-E/E_c)$, is also tested. The background photon fields are the same as model A, and the derived model parameters are listed in Table 3. We found that the cutoff energy of electrons E_c can not be well constrained due to the hard X-ray spectrum. Based on the reduced χ^2 values, the BPL spectrum is better to describe the broadband radiation from HESS J1356-645, which differs from the results by H. E. S. S. Collaboration et al. (2011), and this can be attributed to the revised GeV observation data in this work.

Most of the pulsar rotational energy budget can be roughly estimated with $E_{\text{rot}} = \dot{E}_0 \tau_0 (n - 1)/2$ (H. E. S. S. Collaboration et al. 2018). With the braking index of $n = 3.0$ and the initial spin-down time-scale with a typical value of $\tau_0 = 1$ kyr, E_{rot} is calculated to be about 5.2×10^{48} erg. Compared with the value of W_e in model A, the efficiency of spin-down energy converted into relativistic electrons need to be $\sim 10\%$. It should be noted that the uncertainty of braking index and the unknown initial spin period P_0 or τ_0 of PSR J1357-6429 would result in the uncertainties of E_{rot} and the lepton conversion efficiency. Furthermore, the GeV gamma-ray luminosity of HESS J1356-645 is $L_{10-1000 \text{ GeV}} \approx 1.9 \times 10^{34} (d/2.5 \text{ kpc})^2 \text{ erg s}^{-1}$, and the corresponding gamma-ray efficiency is $\eta_\gamma \approx 0.6\%$, which is comparable with the typical PWNe efficiencies observed at GeV energies (Acero et al. 2013). The X-ray and the TeV luminosities are calculated to be $L_X \approx 5.9 \times 10^{33} (d/2.5 \text{ kpc})^2 \text{ erg s}^{-1}$ (Izawa et al. 2015), $L_{\text{TeV}} \approx 6.0 \times 10^{33} (d/2.5 \text{ kpc})^2 \text{ erg s}^{-1}$ (H. E. S. S. Collaboration et al. 2011), respectively. And H. E. S. S. Collaboration et al. (2018) presents the new result of $L_{1-10 \text{ TeV}} = (14.7 \pm 1.4) \times 10^{33} (d/2.5 \text{ kpc})^2 \text{ erg s}^{-1}$ in the energy range of 1 - 10 TeV. The ratio of $L_{\text{GeV}}/L_{\text{TeV}}$ is ~ 3.2 and $L_{\text{GeV}}/L_{1-10 \text{ TeV}}$ is ~ 1.3 , which are consistent with the mean value of $\sim 2.7^{+2.7}_{-1.4}$ for PWNe, and the ratio of $L_{\text{GeV}}/L_X \sim 3$ is also within the range of other PWNe (Acero et al. 2013). All these characteristics strengthen the PWN scenario for HESS J1356-645.

Xin et al. (2018) performed a comparison of multi-wavelength data of several PWNe, and the gamma-ray spectrum of HESS J1356-645 is similar to HESS J1640-465 (H. E. S. S. Collaboration et al. 2014; Xin et al. 2018), MSH 15-52 (Aharonian et al. 2005; Abdo et al. 2010), HESS J1825-137 (Aharonian et al. 2006; Grondin et al. 2011), and HESS J1303-631 (H. E. S. S. Collaboration et al. 2012; Acero et al. 2013), all of which have the hard GeV spectra with the gamma-ray peak at ~ 100 GeV.

As mentioned in Section 2.1.1, there is evidence that the morphology of the GeV emission from HESS J1356-645 varies with energies. The gamma-ray emission in lower energy band is spatially consistent with the radio nebula, while the gamma-ray emission above 100 GeV shows a different morphology, which is similar to what is observed in the PWN Vela-X (Grondin et al. 2013; Tibaldo et al. 2018). The energy-dependent morphologies could be produced by the different electron populations. The gamma rays with lower energy could be dominated by an older electron population accelerated in the early phase of evolution of pulsar, and the higher energy component may be from the electrons accelerated recently. However, there is no significant difference of GeV spectral indices between the two energy ranges, which is a challenge to such a scenario. In addition, the centroids of the gamma-ray emission in both energy ranges are offset from pulsar, and such offsets are also detected in several gamma-ray PWNe, e.g., HESS J1303-631 (H. E. S. S. Collaboration et al. 2012), Vela-X (Grondin et al. 2013), HESS J1640-465 (Xin et al. 2018). The offset may be caused by the high proper motion of PSR J1357-6429 (Danilenko et al. 2012). Considering the GeV gamma-ray emission from HESS J1356-645 is not significant enough to perform a more detailed analysis, the future multi-band observations are desired to explore the energy-dependent behavior of HESS J1356-645.

4. CONCLUSION

In this paper, we report the significant GeV gamma-ray emission from HESS J1356-645 with more than 13 years of *Fermi*-LAT observation data. The GeV gamma-ray emission from HESS J1356-645 can be described by a 2D Gaussian spatial template, and the spectrum can be fitted by a power law with an index of $\Gamma = 1.51 \pm 0.10$. The gamma-ray characteristics of HESS J1356-645 is similar to several PWNe, such as Vela-X, HESS J1825-137, HESS J1303-631 and MSH 15-52. A leptonic model with a broken power-law spectrum can reproduce the multi-wavelength data of HESS J1356-645. In addition, we found the evidence that the GeV gamma-ray morphology of HESS J1356-645 varies with

energies. And more broadband observations in future are necessary to study the energy-dependent behavior of HESS J1356-645.

1 We would like to thank the anonymous referee for very helpful comments, which help to improve the paper. This
 2 work is supported by the Natural Science Foundation for Young Scholars of Sichuan Province, China (No. 2022NS-
 3 FSC1808), the Department of Science and Technology of Sichuan Province (No. 2020YFSY0016), the Fundamental
 4 Research Funds for the Central Universities (No. 2682021CX074, No. 2682021CX073, No. 2682022ZTPY013), the
 5 National Natural Science Foundation of China under the grants 12103040 and 12147208, the National Key R&D pro-
 6 gram of China under the grant Nos. 2018YFA0404201, G2021166002L, and 2018YFA0404203, NSFC grants U1931204,
 7 11947404 and 11761131007, DFG Sino-German Collaboration Project Nos. BU 777/15-1 and MU 4255/1-1, Depart-
 8 ment of Science.

REFERENCES

- Abdo, A. A., Ackermann, M., Ajello, M., et al. 2010, *ApJ*, 714, 927, doi: [10.1088/0004-637X/714/1/927](https://doi.org/10.1088/0004-637X/714/1/927)
- Acero, F., Ackermann, M., Ajello, M., et al. 2013, *ApJ*, 773, 77, doi: [10.1088/0004-637X/773/1/77](https://doi.org/10.1088/0004-637X/773/1/77)
- Ackermann, M., Ajello, M., Baldini, L., et al. 2017, *ApJ*, 843, 139, doi: [10.3847/1538-4357/aa775a](https://doi.org/10.3847/1538-4357/aa775a)
- Aharonian, F., Akhperjanian, A. G., Aye, K. M., et al. 2005, *A&A*, 435, L17, doi: [10.1051/0004-6361:200500105](https://doi.org/10.1051/0004-6361:200500105)
- Aharonian, F., Akhperjanian, A. G., Bazer-Bachi, A. R., et al. 2006, *A&A*, 460, 365, doi: [10.1051/0004-6361:20065546](https://doi.org/10.1051/0004-6361:20065546)
- Akaike, H. 1974, *IEEE Transactions on Automatic Control*, 19, 716
- Bucciantini, N., Arons, J., & Amato, E. 2011, *MNRAS*, 410, 381, doi: [10.1111/j.1365-2966.2010.17449.x](https://doi.org/10.1111/j.1365-2966.2010.17449.x)
- Camilo, F., Manchester, R. N., Lyne, A. G., et al. 2004, *ApJL*, 611, L25, doi: [10.1086/423620](https://doi.org/10.1086/423620)
- Cao, Z., Aharonian, F. A., An, Q., et al. 2021, *Nature*, 594, 33, doi: [10.1038/s41586-021-03498-z](https://doi.org/10.1038/s41586-021-03498-z)
- Chang, C., Pavlov, G. G., Kargaltsev, O., & Shibano, Y. A. 2012, *ApJ*, 744, 81, doi: [10.1088/0004-637X/744/2/81](https://doi.org/10.1088/0004-637X/744/2/81)
- Danilenko, A., Kirichenko, A., Mennickent, R. E., et al. 2012, *A&A*, 540, A28, doi: [10.1051/0004-6361/201118591](https://doi.org/10.1051/0004-6361/201118591)
- de Jager, O. C. 2008, *ApJL*, 678, L113, doi: [10.1086/588283](https://doi.org/10.1086/588283)
- Duncan, A. R., Stewart, R. T., Haynes, R. F., & Jones, K. L. 1997, *MNRAS*, 287, 722, doi: [10.1093/mnras/287.4.722](https://doi.org/10.1093/mnras/287.4.722)
- Esposito, P., Tiengo, A., de Luca, A., & Mattana, F. 2007, *A&A*, 467, L45, doi: [10.1051/0004-6361:20077480](https://doi.org/10.1051/0004-6361:20077480)
- Fermi-LAT collaboration, :, Abdollahi, S., et al. 2022, arXiv e-prints, arXiv:2201.11184, <https://arxiv.org/abs/2201.11184>
- Gaensler, B. M., & Slane, P. O. 2006, *ARA&A*, 44, 17, doi: [10.1146/annurev.astro.44.051905.092528](https://doi.org/10.1146/annurev.astro.44.051905.092528)
- Green, D. A. 2009, *Bulletin of the Astronomical Society of India*, 37, 45. <https://arxiv.org/abs/0905.3699>
- Griffith, M. R., & Wright, A. E. 1993, *AJ*, 105, 1666, doi: [10.1086/116545](https://doi.org/10.1086/116545)
- Grondin, M. H., Romani, R. W., Lemoine-Goumard, M., et al. 2013, *ApJ*, 774, 110, doi: [10.1088/0004-637X/774/2/110](https://doi.org/10.1088/0004-637X/774/2/110)
- Grondin, M. H., Funk, S., Lemoine-Goumard, M., et al. 2011, *ApJ*, 738, 42, doi: [10.1088/0004-637X/738/1/42](https://doi.org/10.1088/0004-637X/738/1/42)
- H. E. S. S. Collaboration, Abramowski, A., Acero, F., et al. 2011, *A&A*, 533, A103, doi: [10.1051/0004-6361/201117445](https://doi.org/10.1051/0004-6361/201117445)
- . 2012, *A&A*, 548, A46, doi: [10.1051/0004-6361/201219814](https://doi.org/10.1051/0004-6361/201219814)
- H. E. S. S. Collaboration, Abramowski, A., Aharonian, F., et al. 2014, *MNRAS*, 441, 3640, doi: [10.1093/mnras/stu826](https://doi.org/10.1093/mnras/stu826)
- H. E. S. S. Collaboration, Abdalla, H., Abramowski, A., et al. 2018, *A&A*, 612, A2, doi: [10.1051/0004-6361/201629377](https://doi.org/10.1051/0004-6361/201629377)
- Izawa, M., Dotani, T., Fujinaga, T., et al. 2015, *PASJ*, 67, 43, doi: [10.1093/pasj/psv013](https://doi.org/10.1093/pasj/psv013)
- Kirichenko, A., Shibano, Y., Shternin, P., et al. 2015, *MNRAS*, 452, 3273, doi: [10.1093/mnras/stv1420](https://doi.org/10.1093/mnras/stv1420)
- Lemoine-Goumard, M., Zavlin, V. E., Grondin, M. H., et al. 2011, *A&A*, 533, A102, doi: [10.1051/0004-6361/201117413](https://doi.org/10.1051/0004-6361/201117413)
- Mattana, F., Falanga, M., Götz, D., et al. 2009, *ApJ*, 694, 12, doi: [10.1088/0004-637X/694/1/12](https://doi.org/10.1088/0004-637X/694/1/12)
- Murphy, T., Mauch, T., Green, A., et al. 2007, *VizieR Online Data Catalog*, VIII/82
- Renaud, M., Hoppe, S., Komin, N., et al. 2008, in *American Institute of Physics Conference Series*, Vol. 1085, American Institute of Physics Conference Series, ed. F. A. Aharonian, W. Hofmann, & F. Rieger, 285–288, doi: [10.1063/1.3076661](https://doi.org/10.1063/1.3076661)

- Sironi, L., Keshet, U., & Lemoine, M. 2015, *SSRv*, 191, 519, doi: [10.1007/s11214-015-0181-8](https://doi.org/10.1007/s11214-015-0181-8)
- Tibaldo, L., Zanin, R., Faggioli, G., et al. 2018, *A&A*, 617, A78, doi: [10.1051/0004-6361/201833356](https://doi.org/10.1051/0004-6361/201833356)
- Torres, D. F., Cillis, A., Martín, J., & de Oña Wilhelmi, E. 2014, *Journal of High Energy Astrophysics*, 1, 31, doi: [10.1016/j.jheap.2014.02.001](https://doi.org/10.1016/j.jheap.2014.02.001)
- Wood, M., Caputo, R., Charles, E., et al. 2017, in *International Cosmic Ray Conference*, Vol. 301, 35th International Cosmic Ray Conference (ICRC2017), 824. <https://arxiv.org/abs/1707.09551>
- Xin, Y.-L., Liao, N.-H., Guo, X.-L., et al. 2018, *ApJ*, 867, 55, doi: [10.3847/1538-4357/aae313](https://doi.org/10.3847/1538-4357/aae313)
- Zabalza, V. 2015, in *International Cosmic Ray Conference*, Vol. 34, 34th International Cosmic Ray Conference (ICRC2015), 922. <https://arxiv.org/abs/1509.03319>
- Zavlin, V. E. 2007, *ApJL*, 665, L143, doi: [10.1086/521300](https://doi.org/10.1086/521300)